L'GARDE
SMART SPACE TECHNOLOGY

L • GARDE INC. CORPORATE PRESENTATION

Inflatable Power Antenna Technology

David Lichodziejewski, Dr. Costa Cassapakis

INFLATABLE POWER ANTENNA TECHNOLOGY

David Lichodziejewski, Dr. Costas Cassapakis, AIAA Members
L'Garde, Inc.
15181 Woodlawn Ave.
Tustin, CA 92780
(714) 259-0771

Abstract

As an alternative to the expensive and environmentally sensitive RTG (Radioisotope Thermal Generators), L'Garde is developing the Power Antenna concept. This new technology utilizes an inflatable reflector to concurrently concentrate solar energy for space electrical power generation, while acting as a large aperture high gain antenna. L'Garde has conducted a detailed study of the issues concerning the design and performance of the Power Antenna concept. Much of the effort was conducted in conjunction with JPL under the Gossamer Spacecraft program. The technical objectives of the Power Antenna program are to reduce the mass and stowage volumes of the Power Antenna. We have optimized the key parameters, and developed an enhanced, state-of-the-art configuration, based on generic mission requirements. A generic Jovian mission resulted in a 6.7m aperture Power Antenna subsystem mass of only 21.9kg yielding 75 watts of electrical power. This low mass yields a power density of 3.42 watts/kg. A state-of-the-art Earth orbiting power subsystem yields a 100 watt/kg. This same system in a Jovian orbit, assuming it retains its conversion efficiencies, would yield about 3.7 watts/kg. The power antenna compares well to this performance, particularly when it is also includes a large aperture high gain antenna shown to exceed mission requirements.

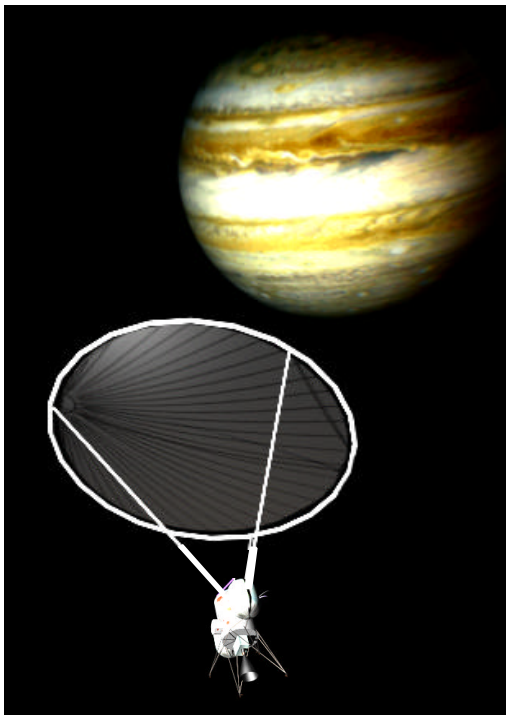

Figure 1. Power Antenna

Power Antenna Concept

The Power Antenna utilizes an inflatable parabolic reflector to concentrate solar energy for space electrical power generation, while acting concurrently or alternatively as a large aperture high gain antenna. First, the parabolic reflector acts as a solar concentrator, focussing solar energy onto an array of photovoltaic (PV) cells for electrical power generation. In deep space ambient sunlight is severely diminished and a concentrator is required to increase the light intensity levels for efficient use with conventional solar cells. Second, a beam splitter or metallic grid is mounted in front of the solar cell array to deflect Radio Frequency (RF) energy onto a feed (Figure 2). In this way the optical and RF energy impinging on the reflector can be separated and utilized for deep space power generation and/or high gain RF communications.

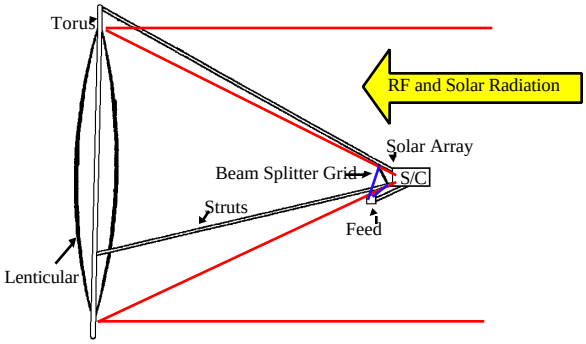

Figure 2. Power Antenna Schematic

Reflector Design and Construction

A series of low film stress reflectors were designed using FLATE, a L'Garde gore design tool, and analyzed using FAIM (1), a L'Garde FEA code for analyzing inflatable structures.

FLATE is used to solve the inverse problem of determining a flat gore shape, such that when the reflector is constructed and inflated to a specified pressure it forms a paraboloid. The code uses the desired shape and material properties to determine the flat gore shape. A FLATE output gore shape for the 350 psi, 1m, F/D 1.0 reflector is shown in Figure 3. The waviness in the gore outline is inherent in the plotting routine, the actual gore edges are smooth.

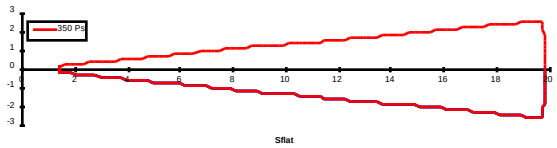

Figure 3. Power Antenna Gore Layout

Shown in Figure 4 is the FAIM result for the medium film stress (350psi) gore. Please note this is a half gore model. To minimize FAIM computer time all symmetry is utilized. To construct the full reflector the gore is first mirrored around its centerline, and then repeatedly mirrored to represent the full reflector. The color bands represent the delta from a best fit parabola. The most pronounced differences are found near the gore ends and are up to 10.48*10-3 in. or .27 mm from the best fit paraboloid. Fortunately these areas are very small and the calculated RMS accuracy over the full reflector surface is 0.071 mm. This precision is theroetical and does not include material inconsistencies and manufacturing tolerances. A similar analysis was conducted at the other pressures.

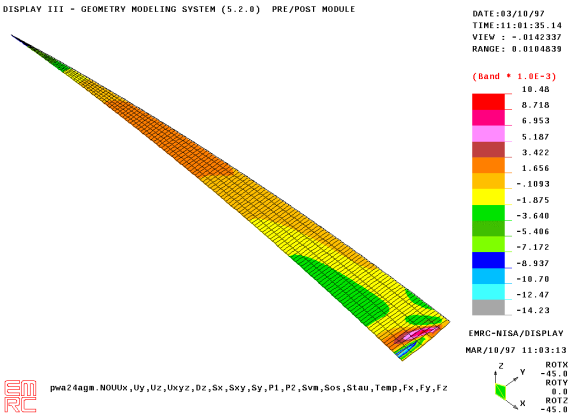

Figure 4. FAIM Half Gore Model

The main requirement for the canopy (which, with the reflector completes the lenticular structure) is that of high optical transmissivity. It must of course also provide a low permeability membrane to contain the gas. The surface precision requirements are not as strict as that of the reflector. We decided to use the same gore template to cut the canopy gores. The modulus of Mylar is 540,000 psi, similar to that of Kapton. Were surface accuracy of the canopy a factor, we would re-design the gore shapes to compensate for the different modulus. However, for the Power Antenna canopy we used the gore shapes designed for the reflector.

When completed the canopy was mounted to the canopy rim and attached to the tub using quarter turn latches. The completed canopy mounted to the solar test fixture is shown below in Figure 5. The canopy is shown here during setup (below its operating pressure), at its proper operating pressure it is considerably less wrinkled

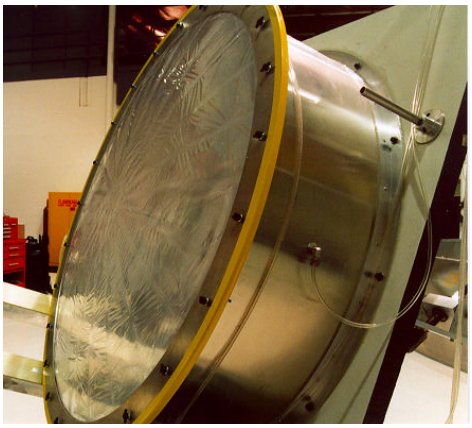

Figure 5. Canopy Mounted on the Solar Test Stand

Reflector Surface Precision Measurements

Surface accuracy measurements of the reflectors were conducted using the V-Stars (2) video-grammetry system. The system uses a high-resolution digital camera and software to measure the surface accuracy of the reflector. One of a series of pictures used in the measurement is shown below in Figure 6. The optical targets used to locate positions are visible as bright white dots. Visible on the lower right portion of the rim is a geometrically precise bar with targets on the ends used as a reference for the photo-grammetry algorithm. Other references visible are the four targets arranged in a cruciform arrangement toward the lower left. Note, the DCS 460 used by the V-Stars system is black and white only. Color is not required to measure surface accuracy and was sacrificed to provide a higher resolution imager chip.

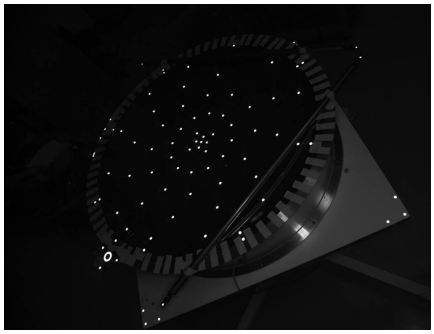

Figure 6. V-Stars Photograph

Shown in Figure 7 are the reflector surface precision measurements for the wrinkled reflectors at 3 different pressures. The surface data from V-Stars was put into a best-fit paraboloid fitting routine. The relatively small distortions from the expected parabola are caused by manufacturing, material, design errors, and rim offsets. Also shown below are the RMS surface precision errors. Accuracies below 1.0 mm are considered excellent.

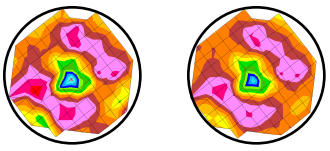

Figure 7. Measured Reflector Precision

SOLAR TESTING

A new photographic method has been researched and developed to characterize the Power Antenna reflectors and is described briefly below. This technique uses a high-resolution highly calibrated CCD camera to photograph the Sun's image cast by the concentrator. With these images and software the performance of the reflector can be discerned, documented, and compared. The effect of materials, film stress, reflector configuration, and canopy can be viewed directly and the data used to optimize the Power Antenna configuration.

The photographic method uses a Kodak/Nikon 460 digital camera to photograph the reflection of the sunlight concentrated by the reflectors on the target. A water-cooled target is mounted near the focal plane of the reflector. The target is movable so as to traverse the planes of interest near the focal point. Various filters were placed over the camera so as not to saturate the image at the high intensities expected. The resulting digital images were high resolution with the values of the pixels representing the intensities of reflected light

The camera is mounted near the edge of the reflector and has an oblique view of the target. Software has been developed that electronically rotates the image into a normal plane and adjusts the perspective. Once this normalization is complete the value of each pixel is run though a calibration curve and the image plotted on a contour plot. Software was also developed that allows us to define areas of the image for concentration ratio calculations.

The data reduction flow diagram is shown in Figure 8. The picture at the top left is an actual datapoint from the Power Antenna. There is a heavy filter on the lens so as not to overexpose the frame. The edge of the target is visible as a hazy ellipse in the middle of the picture. The first process in the data reduction is the perspective change algorithm. This routine down-samples the image and electronically rotates it into a normal perspective. The target image is now circular. After the perspective change the image is "gamma corrected", this correction uses the camera calibration and corrects the pixel intensities to be linear with light intensity. The data is then corrected for ambient conditions to produce a concentration ratio. Contour plots of the corrected data are produced for comparison. Another routine was written to produce the familiar intensity plots shown on the bottom left. This routine finds the "centroid" of the concentrated energy and sweeps a radius around this point and averages the intensity within various radii to generate the shown plot. This plot is a 2-dimensional representation of the image. As it is seen in the contour plots the image is not axisymmetric. The intensity plot is a very convenient way to characterize and compare images but it does not fully represent the concentrated image.

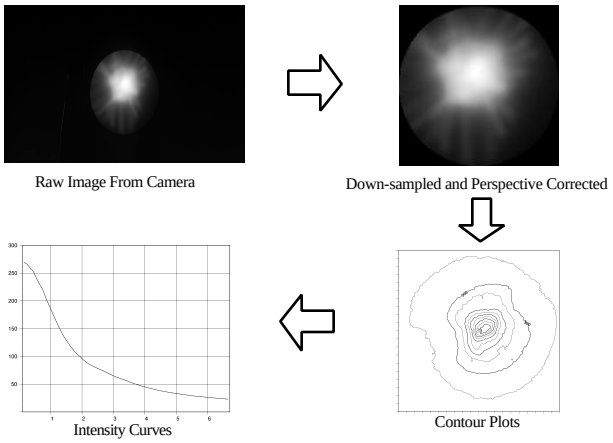

Figure 8. Solar Test Data Reduction Technique

Test Technique

A picture of the functioning test stand is shown in Figure 9. Visible in this picture are the hoses used to supply cooling water to the target. One hose is connected to a faucet and the other vents to a drain. There is a thermo-couple mounted behind the target face to measure temperature. Tests were conducted to determine the proper cooling flow and at this flow level it was found the target stays relatively cool. On a cloudless summer day only a trickle of water was required to keep the target under 100F. Equilibrium temperature with the flow off was not much higher. There is enough convection, conduction, and radiation to keep the target cool.

Figure 9. Functioning Test Stand

A picture of the concentrated sunlight is shown in Figure 10. The target brightness appeared much brighter in person than it does in the photo. It was not possible to view the spot for any length of time with the naked eye, and welding goggles were required.

Figure 10. Concentrated Energy

Another view of the test stand is shown in Figure 11. Visible at the lower left of the reflector is the camera used to acquire the images. The oblique view the camera has of the target is shown. To keep the view angle the camera has to the target constant the camera is translated back and forth with the target. The slot used to relocate the camera is just visible at its base. Also note the white covering material surrounding the camera used to keep it cool during testing.

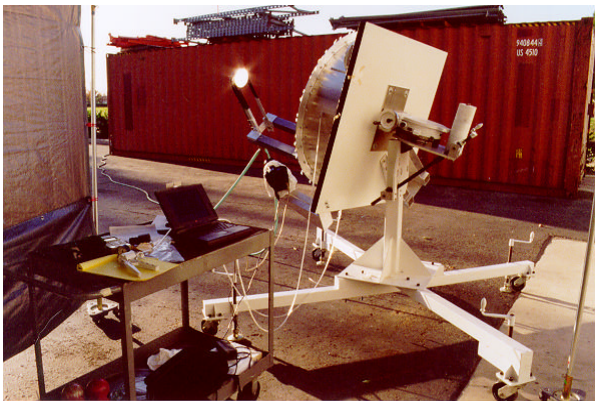

Figure 11. Test Equipment

SOLAR TESTING DATA ANALYSIS

Shown in Figure 12 are the results of film stress on the reflected image. All measurements are performed on 1m reflectors using the sun as the source, concentration ratios are considerable higher at larger apertures. The highest concentration ratios measured were on the 600 psi film stress reflector which had the narrowest and highest intensity image. The 350 psi film stress reflector had a more diffuse and lower intensity reflection, with the 100 psi film stress reflector lower still. Note, however, that in the 100 psi case the maximum intensities are lower but further away from the target center they are higher. The light concentrated by the lower film stress reflector is a lower overall intensity but scattered over a larger area. Increasing film stress pulls out wrinkles in the material and results in a more specular reflection.

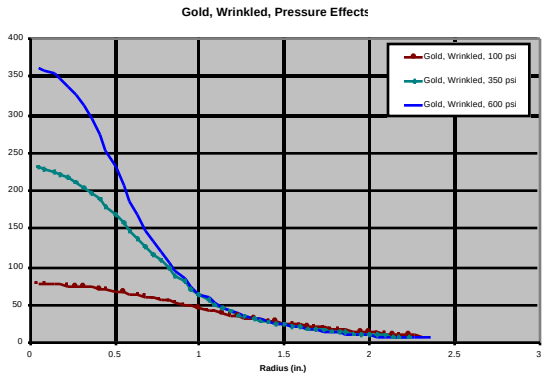

Figure 12. Effect of Pressure

Many reflector configurations were tested. Other than pressure effects there are the effects of material wrinkling and the canopy. Shown in Figure 13 are some of the configuration effects. The highest intensities measured are just below 400 suns for the 600 psi unwrinkled reflector. The next highest intensities measured (of around 360 suns) were for the same reflector but in a deliberately wrinkled state. The reflector was folded in a manner representative of a packaged reflector and stored in a compressed state overnight. The effect, not surprisingly, is to scatter the image somewhat. The effect of the canopy is quite pronounced and significantly reduces the concentration ratios. Interestingly, the image passed through the canopy is not scattered very much and still falls in a 1" radius of the target center. The image is very attenuated with much of the light completely reflected away from the target. The effect of wrinkling with the canopy is similar to that measured without the canopy, and not a large effect.

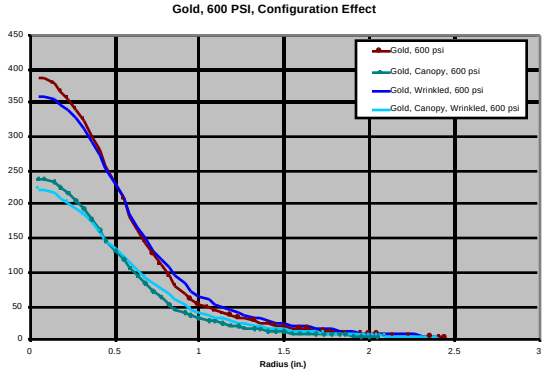

Figure 13. Effect of Configuration

Correlating all canopy data the losses are much higher than expected. A correlation of all known canopy effects results in a two-pass canopy transmission of only 62% or a one pass of %79. The effect is similar for all film stresses and configurations. The measured transmissivity of the canopy was 90%. The canopy has seams which doubles up the material in a few areas. Accounting for the seams results in an overall transmissivity of 88.2%. The transmissivity of the Mylar canopy film is also a function of the incident angle of the light ray. When a light ray hits the canopy at a very oblique angle more energy is reflected away, this effect is quite pronounced around the edge of the reflector where the incident angles are quite large. A second scattering of light could be caused by wrinkles in the canopy itself. It is believed the losses are attributable to synergism between these two factors.

Shown in Figure 14 are the effects at different focal planes. The highest concentration ratios measured often occurred just off the expected focal point. In this case the most focussed image occurred 0.5" forward of the expected focal point. This was attributed to inaccuracies in the measuring system used to find the focal plane. As expected the highest intensities are measure on or near the focal point and drop off quickly away from the focal plane. Since the Power Antenna concept uses a PV array as the primary conversion method it is expected we will want to use off focal plane conditions to provide a large, diffuse image for the array (see Ref. 3). For this reason a complete set of off focal plane measurements were conducted for the test matrix.

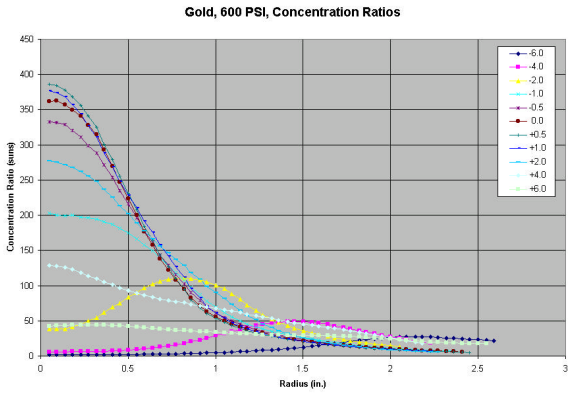

Figure 14. Effect of Focal Plane

RAY TRACING

The main goal of the Power Antenna program is a system study to optimize the reflector configuration. Since we are unable to ground test the large aperture (6m) reflectors it is important to utilize the solar test data to calibrate our ray-tracing techniques. In this way we can develop credible optical performance estimates for larger reflectors.

In order to model the surface errors associated with wrinkling, a mathematical technique was incorporated into the ray tracing code. While the code is calculating what direction an incident light ray will be reflected a slight error is introduced using a "Monte Carlo"

statistical technique. The error is in two parts, the magnitude of the direction error, and the direction of the error. An RMS slope error of s milli-radians means that the angle q the reflected ray makes with the "errorless" reflector direction has an average value of zero (along the errorless direction) and a standard deviation of s The angle q is assumed to be Gaussian-distributed. On the other hand, the azimuth angle around the "errorless direction" on the reflected ray may take is taken to be uniformly distributed. The direction of the error is assigned randomly; the result is the error cone shown in Figure 15.

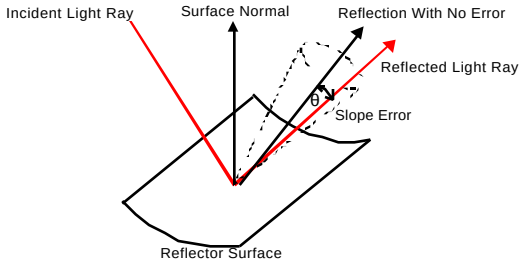

Figure 15. Ray Tracing Slope Error Model

The measured reflector surfaces from the V-stars testing was input into the ray tracing code as was the measured surface reflectivity parameters. RTRACE5, another L'Garde design code, was run with different levels of slope errors in order to calibrate the local slope errors. Some results of this analysis are shown in Figure 16 for the 600 psi film stress case. The measured test data is shown as the solid black line. Ray tracing runs of various slope errors were conducted and plotted. As can be seen the measured data most closely resembles the 2.0 mrad slope error case, interpolating we find a 2.2 mrad slope error. In this way we can determine the proper slope error as a function of film stress.

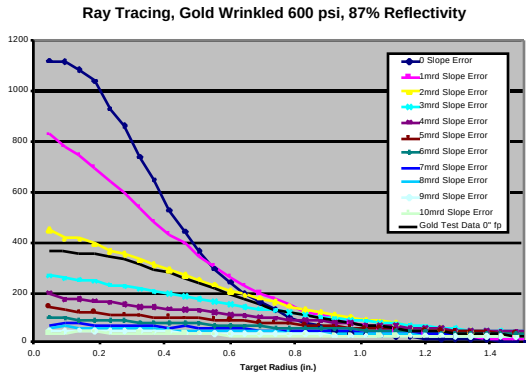

Figure 16. Ray Tracing Calibration

This analysis was conducted for the other film stresses and the results shown in Figure 17. At the lower film stresses the slope errors are quite high as expected. The wrinkled material has a higher slope error than the unwrinkled material. As the film stress is increased however, the slope error decreases. At 600 psi most of the wrinkling is pulled out of the material. The slope error at this point comes from the actual surface roughness of the metalization the global error in the reflector fabrication.

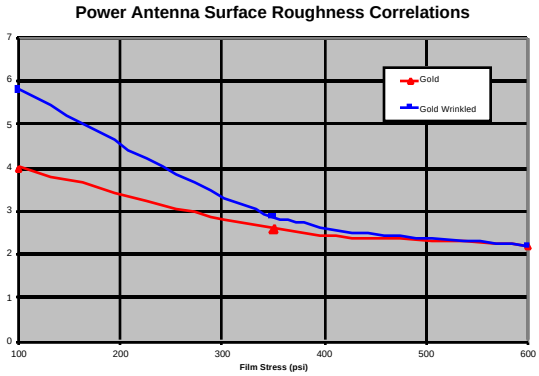

Figure 17. Ray Tracing Surface Correlations

Using the above procedure and test data the ray tracing code has been calibrated to reproduce the measured intensities of inflatable reflectors at different film stresses. The technique will now be used to predict the performance of larger reflectors. Future analysis will assume that though the aperture of the reflector will be increased significantly the local surface errors will not scale but will remain the same, only a function of material and film stress. L'Garde's experience with many reflectors over the years shows this to be true. The wrinkling of the films appears similar regardless of the size of the reflector. Most of the wrinkling occurs during handling of the material and construction of the reflector though some is a function of the packaging concept. The packaging concept will vary with configuration. The Power Antennas were wrinkled using a generic packaging described in the Solar Testing Data Analysis section and therefore represent a deployed on-orbit configuration.

SYSTEM STUDY

The Jovian rendezvous mission was chosen as the design point for optimization. This complemented work conducted under the JPL Gossamer Spacecraft program, which conducted a conceptual design of the configuration during 1997. The Power Antenna optimization is more generic and not as mission specific as the Gossamer Spacecraft project. It is intended chiefly to explore the design sensitivities of the key Power Antenna variables and not to specifically refine a particular mission and bus. However, to confine

the design space to a manageable effort the Jovian rendezvous mission was selected. Where possible any synergism between the two programs has been exploited.

The following mission assumptions were used in calculating the masses of the three Power Antenna study configurations. The main requirement in the Power Antenna is the generation of 75 watts of electricity when the antenna is oriented toward the sun. The reflector is not deployed until fairly close to the Jovian orbit. This assumption was made to be consistent with the mission assumptions made during JPL's Gossamer Spacecraft program and to reduce the complexity of de-focussing the PV array to reduce intensities closer to sun. The mission duration is 12 months after the antenna is inflated. The spacecraft is assumed to be in a sleep state during the flight from Earth to Jupiter powered by batteries and possibly a small PV array mounted directly to the spacecraft. The antenna will be deployed before orbital insertion to provide power and communication for the insertion itself and must withstand the associated forces. Should the forces be higher it is possible to re-inflate the structure briefly to reinforce it for known high load conditions. This, however, is not explored here. The insertion forces are assumed to be 0.05 g's axial to the antenna centerline with ±10 degree thrust vectoring of the nozzle.

Configuration/Deployment

The structural concept is shown in Figure 18, though the dimensions have changed slightly. A circular tube or torus made up of segments of straight tubes supports the lenticular. The torus is attached to the spacecraft by three struts spaced evenly around the circumference of the torus.

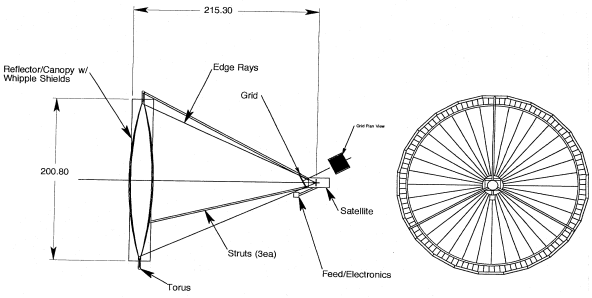

Figure 18. Power Antenna Structural Concept

It is not practical to use a constantly inflated structure for the main structural members of the Power Antenna. In time leaks can develop, and with high internal pressure a tremendous amount of make-up gas would be required to replenish the lost inflatant. Instead a rigidization scheme is used so that the structure can support itself without internal pressure. A rigidizable structure would be deployed using pressurized gas, once it has reached its final geometry it becomes rigid and internal pressure is no longer required.

For deep space missions L'Garde has developed a practical rigidization scheme known as sub T_g (glass transition temperature) rigidization. The structure material is composed of a specially designed elastomeric compound with a T_g well below that of the on-orbit equilibrium temperature of the structure. Prior to deployment the packaged assembly will be at or near the equilibrium temperature of the spacecraft which is generally higher than the deployed equilibrium temperature due to internal electronics and control systems. The material is chosen so that the T_g will be below that of the spacecraft temperature, so the structure will be in its pliable softened state while stowed. The structure is then inflated to reach its final geometry and the pressure is held until the structure cools and becomes rigid. Once the structure is rigidized the pressure is no longer required for strength. Care must be taken not to allow the intense concentrated solar energy from the reflector to wander onto the cold rigidized structure as temporary local "softening" can occur. The possibility of thermal excursions can be minimized through the use of MLI around the cold rigidized structural elements.

The canister and deployment systems are based on the JPL Gossamer Spacecraft program. A picture of the canister concept is shown in Figure 19. This particular canister was designed for a 9m reflector with 300 psi film stress so the tanks are larger than expected. For the 6.7m class reflector however the basic canister design is valid. The L'Garde Deployment Devices (LDDs) deploy the struts in a controlled manner. The three struts are deployed at equal rates, once the struts are fully deployed the torus is inflated and finally the lenticular is brought to it's inflation pressure.

Figure 19. Power Antenna Canister Concept

The Gossamer Spacecraft Power Antenna deployment sequence is shown in Figure 20. The deployment is

initiated on the left with the jettisoning of the canister lid. The lid can be hinged if required. The next picture in the sequence shows the LDDs deploying the struts. Note the torus and lenticular are still uninflated and suspended between the extending struts. The next picture shows the struts at full deployment and the torus partially inflated. The lenticular is still not inflated. Finally the deployment is complete with the inflation of the lenticular.

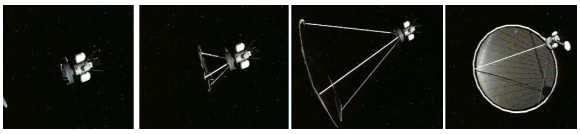

Figure 20. Power Antenna Deployment Sequence (courtesy TDM Inc.)

System Study

The following parameters were traded off for the optimization process, film stress of the reflector membrane, aperture size, and the size of the PV array. Also optimized, are the structural considerations such as torus and strut tube diameter and material thicknesses. Mission parameters such as the loads and accelerations are fixed.

Initially the aperture was sized based on the spacecraft power requirement of 75 watts of electrical power. The optical losses shown in Table 1 were accounted for in the aperture sizing. The Sun's output at Earth's orbit is 1353 watts/m2. At Jupiter's orbit, 5.2 AU away from the Sun, the flux is 50.04 watts/m2. Assuming the losses shown below and the further assumption that about 60% of the energy concentrated by the concentrator will fall on and be usable by the PV array, the total efficiency expected is about 4.77%. To achieve a 75 watt output from the PV array with these efficiencies we need a concentrator with a 33.5 m^2 aperture or 6.5m diameter. It should be noted that this is only the first iteration and that the reflector will be sized again based on the results of this analysis.

Table 1. System Optical Efficiency

Cause	Efficiency
Shadowing by struts (S/C blockage already included)	99%
Light passing through canopy twice	63%
Light passing through meteoroid shield twice	81%
Shadowing by RF grid	90%
Film Reflectivity	85%
Solar cell conversion to electricity	20%
Total Efficiency	7.72%

A technique was developed to analyze PV arrays at different focal planes. Ray-tracing was conducted for each configuration at many focal planes. The technique analyzed each focal plane and chose the plane with the smallest yet most even and diffuse intensity distribution, this plane yielded the lightest and most efficient PV array design and location

Study Results

Ray tracing was conducted on the three configurations and the power generation performance was estimated. For each configuration to generate the required 75watts of on-orbit power the aperture required was 6.7m. An unexpected result of the study was that the power generation is insensitive to the film stress. As the film stress is reduced the concentrated image becomes larger and requires a larger PV array to capture the energy. Some light is scattered by the increased wrinkling but the overall diffusing of the image leaves the PV array illuminated in an even and diffuse manner.

L'Garde has developed a tool to conduct preliminary mass estimates of candidate configurations. This tool was utilized in estimating the masses of the three 6.73m Power Antenna study configurations. The tool sized structural features like torus and strut diameters based on film stress and expected loadings and accelerations. These estimates are based on analytical calculations and compiled L'Garde test data of similar structures and configurations. Further configuration components such as the canister, inflation system, and other equipment masses are based on required packaging volumes, required inflation gas, and empirical data on similar configurations. The results from the sizing analysis are shown in Table 2 and Table 3. The predicted surface precisions for the 100, 350, and 900 psi 6.73m aperture reflectors are 1.9mm, 1.4mm, and 1.3mm RMS respectively. These conservative surface precision estimates are based on extrapolations from the 1m test reflectors. A constructed 6.7m aperture is expected to be about 1mm RMS.

Table 2. Power Antenna System Study Geometries

	100 psi	350 psi	600 psi
Torus Tube Diameter (cm.)	10.2	14.0	16.5
Torus Thickness (mil)	7.0	8.0	10.0
Strut Length (m)	5.5	5.5	5.5
Strut Diameter (cm)	5.3	6.4	6.4
Strut Thickness (mil)	5.0	5.0	5.5
PV Diameter (cm)	97.5	74.7	51.8
Stowed Volume (m^3)	0.12	0.15	0.18

Table 3. Power Antenna System Study Masses

	100 psi	350 psi	600 psi
Reflector/Canopy	1.9	1.9	1.9
Torus	2.8	4.4	6.4
Struts	0.8	0.9	1.0
Attachment Hardware	2.0	2.0	2.0
MLI for inflatable	0.4	0.6	0.6
Inflatant/Makeup gas	1.0	3.1	5.3
Tank for Reflector	0.8	2.6	4.3
Inflation System	2.0	2.0	2.0
Canister	9.5	11.9	14.0
PV Array	0.7	0.4	0.2
Total (kg)	21.9	29.8	37.9

The reflector and canopy masses are insensitive to

internal pressure, as the membranes are the same for all configurations. A large change in mass is noted in the torus, as the increased internal pressure results directly in compressive loads in the torus (Table 3 right side). The torus tube diameter must be increased to withstand the added loads. The material properties of the cold rigidized structure are derived from L'Garde test data and theory. The struts are also effected by the internal pressure in that they must support the added mass of the torus both in compression and bending during orbital maneuvering.

The masses of the Inflatant and tanks are, as expected, a strong function of internal pressures. The leak rate of the gas due to micrometeoroid damage is a strong function of the internal pressure. The make-up gas masses are calculated using two L'Garde codes, ROID and GAS. ROID, given the expected micrometeoroid flux (in our case a flux similar to Earth's geosynchronous orbit was applied) and the geometry of the reflector, calculates the area of the holes caused by the micrometeoroids as a function of time on orbit. ROID uses data gathered on film damage during impact tests of small particles on thin membranes to calculate the effect of the micrometeoroid flux on the lenticular. The particles tested represent the size and velocities of micrometeoroids found on orbit. Once the size and number of the holes generated on orbit are calculated as a function of time, GAS calculates how much gas will leak from the reflector given the specified internal pressure. Once the mass of the make-up gas is calculated a tank mass is estimated using the most efficient composite tanks available. The results are the make-up gas and tank masses shown in Table 3.

Optical testing shows that the size and mass of the PV array necessary to collect the required 75 watts is inversely affected by the internal pressure, the effect was included in the system study. Thus, the lower film stresses have larger arrays and an associated mass penalty. The array sizes were based on the PV array design philosophy documented in the previous section. The masses were estimated by assuming a 0.94 kg/m2 areal density of the array. This density is based on other work L'Garde has conducted into deep space probes. The mass estimate is for a 4 mil thick crystalline silicon cell with 3 mils of cover glass to protect it from the space environment. The estimate also includes adhesives and connections. It is assumed the cells are mounted directly to the spacecraft and need no further substrates. Certainly, more detailed design work must be conducted to fully define the array concept, however this simple design philosophy captures the mass sensitivities between the various configurations.

SUMMARY AND CONCLUSIONS

During the SBIR Phase II of the Power Antenna program L'Garde has conducted a detailed study of the issues concerning the design and performance of the Power Antenna concept. Key parameters influencing the concept design were identified and quantified through testing and analysis.

Much design information resulted during the optical testing of the reflectors and subsequent data analysis. Reduction of internal pressure in the lenticular results in diffusing the projected image. This diffusion stems from increased surface wrinkling in the reflector material. The diffusion enlarges the image but does not scatter much light off the target, as expected. By enlarging the target region slightly, most of the incident light can still be captured. This conclusion was further confirmed by the system study, which showed a pronounced insensitivity to the reduction in film stress. Had the optical energy been severely scattered it would have missed even an enlarged target altogether and rendered the configuration less efficient.

Optical losses through the canopy were larger than predicted. A two-pass transmission through the canopy was estimated at 81% ($90\%^2$) yet a survey of the optical test data yielded a two-pass transmissivity of 63% less than expected and a significant system loss. The effect is believed to be due to high incidence angles of the incoming and reflected light rays. These losses were carried into the system study for conservatism but it is firmly believed the canopy performance can be improved through the use of anti-reflective coatings.

Calibration of the ray tracing methods to enhance accuracy proved to work very well. The simple wrinkle error model documented above was able to match the test data with surprising accuracy. The effects of thermal gradients on the reflector surface precision were not evaluated during the system study and that these effects can adversely influence optical performance. Thermal gradients, however, can be significantly reduced through the use of thermal coatings, and that conservatism in the surface precision predictions will accommodate these effects.

An RF analysis not documented in this paper was conducted that showed all reflectors exceeded the required 48.7dB gain, for good uplink/downlink with Earth, with some margin.

Results of the solar testing system study validate our prediction that the lightest system masses occur at the lowest film stress configurations. In fact dropping the reflector film stress from 600 to 100 psi can cut the system weight almost in half yet still produce the same power output. This is due in no small part to the use of a PV array as the energy conversion method. The diffusion of the image with reduced lenticular pressures eminently complements the PV requirement of a

homogeneous luminous intensity profile.

The generic Jovian mission resulted in a Power Antenna subsystem mass of only 21.9kg. well within the realm of the micro-spacecraft arena, able to benefit most from its economies. This low mass yields a power density of 3.42 watts/kg. A state-of-the-art Earth orbiting system yields 100 watt/kg. of solar power. That same system in a Jovian orbit, assuming it retains its conversion efficiencies at the reduced temperatures and light intensities would yield about 3.7 watts/kg. The power antenna compares well to this performance, particularly when it includes a large aperture high gain antenna shown to exceed mission requirements.

The low cost, light weight, reliable, and environmentally benign Power Antenna concept, concurrently providing high bandwidth communications, reliable space power and thermal energy, make this an eminently enabling technology in the field of deep space probes and interplanetary travel. This new technology will allow the space community to meet the challenge of reducing mass, volume, and most importantly, the price of spacecraft and launch vehicles of the future.

ACKNOWLEDGEMENTS

The authors are indebted to Bill Nesmith of JPL, the SBIR technical monitor, for his overall guidance of the program and his expertise in the field of space power. Also, to Dr. Joel Sercel and the JPL Gossamer Spacecraft team for their enthusiasm and involvement.

REFERENCES

1. Palisoc, A. L. and Huang, Y., "Design Tool for Inflatable Space Structures", AIAA-97-1378 Proc. 38th AIAA/ASME/ASCE/AHS/ASC Structures, Structural Dynamics, and Materials Conference, Kissimmee, FL, April 9-10, 1997.

2. VSTARS A video-grammetric measurement technique by Geodetic Services Inc., 1511 S. Riverview Dr., Melbourne, FL 32901.

3. Cassapakis, C. and Thomas, M; "A Power Antenna for Deep Space Missions", Solar Engineering, ASME, Book H01046, 1996

4. Cassapakis, C. and Thomas, M; "Inflatable Structures Technology Development Overview" AIAA 95-338, 1995 Space Programs and Technologies Conference, September 26-28, Huntsville, AL.

5. M. Thomas and G. Veal, "Scaling Characteristics of Inflatable Paraboloid Concentrators" Solar Engineering, ASME, Book No. H00630, 1991.

6. R.E Freeland and G. Bilyeu (1992). "IN-STEP Inflatable Antenna Experiment," 43rd Congress of the International Astronautical Federation, Paper IAF-92-0301.

7. M. Thomas and G. Veal, "Highly Accurate Inflatable Reflectors," Report AFRPL TR-84-021, May 1984. (AD-A143628)

8. G. R. Veal, "Highly Accurate Inflatable Reflectors, Phase II," Report AFRPL TR-86-089, March 1987 AD-B111435.

L•Garde Inc
15181 Woodlawn Avenue
Tustin, CA 92780-6487
www.LGarde.com